PROCEEDINGS OF SPIE

Tissue temperature monitoring using thermoacoustic and photoacoustic techniques

Manojit Pramanik, Todd N. Erpelding, Ladislav Jankovic, Lihong V. Wang

SPIE.

Tissue temperature monitoring using thermoacoustic and photoacoustic techniques

Manojit Pramanik[1], Todd N. Erpelding[2], Ladislav Jankovic[2], and Lihong V. Wang[1*]

[1]Optical Imaging Laboratory, Department of Biomedical Engineering, Washington University in St. Louis, St. Louis, MO, USA 63130;
[2]Philips Research North America, Briarcliff Manor, NY, USA 10510

ABSTRACT

Real-time temperature monitoring with high spatial resolution (~1 mm) and high temperature sensitivity (1 ^{o}C or better) is needed for the safe deposition of heat energy in surrounding healthy tissue and efficient destruction of tumor and abnormal cells during thermotherapy. A temperature sensing technique using thermoacoustic and photoacoustic measurements combined with a clinical Philips ultrasound imaging system (iU22) has been explored in this study. Using a tissue phantom, this noninvasive method has been demonstrated to have high temporal resolution and temperature sensitivity. Because both photoacoustic and thermoacoustic signal amplitudes depend on the temperature of the source object, the signal amplitudes can be used to monitor the temperature. The signal is proportional to the dimensionless Grueneisen parameter of the object, which in turn varies with the temperature of the object. A temperature sensitivity of 0.5 ^{o}C was obtained at a temporal resolution as short as 3.6 s with 50 signal averages.

Keywords: thermoacoustics, photoacoustics, temperature sensing, tissue phantom, tissue temperature, ultrasound array system.

1. INTRODUCTION

During thermotherapy or cryotherapy, it is necessary to monitor the temperature distribution in tissues for the safe deposition of heat energy in the surrounding healthy tissue and efficient destruction of tumor and abnormal cells. To this end, real-time temperature monitoring with high spatial resolution (~1 mm) and high temperature sensitivity (1 ^{o}C or better) is needed.[1] The most accurate temperature monitoring is by directly measuring the temperature with a thermocouple or thermistor. However, it is invasive, hence generally not preferred and often not feasible. Several noninvasive temperature monitoring methods have been developed. Infrared thermography is a real-time method with 0.1 ^{o}C accuracy but is limited only to superficial layers.[2] Ultrasound can be applied for real-time temperature measurements with good spatial resolution and high penetration depth, but the temperature sensitivity is low.[3-5] Magnetic resonance imaging has the advantages of high resolution and sensitivity, but it is expensive, bulky, and slow.[6,7] Therefore, an accurate, noninvasive, real-time temperature measurement method needs to be developed.

The thermoacoustic (TA) and photoacoustic (PA) effects are based on the generation of pressure waves on absorption of microwave and light energy, respectively. A short microwave or laser pulse is usually used to irradiate the tissue. If thermal confinement and stress confinement conditions are met, then pressure waves are generated efficiently. The pressure rise of the generated acoustic wave is proportional to a dimensionless parameter called the Grueneisen parameter, and to the local fluence. The local fluence depends on the tissue parameters, such as the absorption coefficient, scattering coefficient, and anisotropy factor, and does not change significantly with temperature. However, the Grueneisen parameter, which depends on the isothermal compressibility; the thermal coefficient of volume expansion; the mass density; and the specific heat capacity at constant volume of the tissue; changes significantly with temperature. Thus, the generated TA/PA signal amplitude changes with temperature. Here, we show that by monitoring the change in the TA/PA signal amplitude, we were able to monitor the change in temperature of the object.

---

[*] Email: lhwang@biomed.wustl.edu

The TA/PA technique has been widely applied in biomedical imaging applications, such as breast cancer imaging, brain structural and functional imaging, blood-oxygenation and hemoglobin monitoring, tumor angiogenesis, and, recently, for molecular imaging.[8-22] Recently, PA sensing has been used to monitor tissue temperature.[1,23-27] Also, a combined TA/PA temperature sensing technique was recently demonstrated for the first time.[28] These two techniques do not interact and can be used independently. Depending on the need, one can choose which technique to use. The main difference between these two techniques is the contrast mechanism. For example, water and ion concentrations are the main sources of contrast in TA measurements, whereas blood and melanin are the main sources of contrast in PA measurements. Therefore, to monitor blood vessel temperature, the PA technique will be more useful; whereas to monitor the temperature of muscles, the TA technique will be preferred. TA/PA temperature sensing is a noninvasive, real-time method. The TA/PA technique has the ability to image deeply (up to 5 cm) with high spatial resolution (scalable: millimeters to microns). Because microwaves penetrate more deeply into tissue than light, we can potentially monitor temperature *in vivo* for locations deep inside the body. Here we report for the first time the use of a clinical ultrasound imaging system to monitor temperature using TA measurements. Parallel detection of TA waves with an ultrasound array transducer improves the imaging frame rate compared to a mechanically-scanned single element transducer. Furthermore, demonstration with an ultrasound imaging system is an important first step towards potential clinical translation.

2. THEORETICAL BACKGROUND

If the microwave/laser excitation is much shorter than both the thermal diffusion (i.e., the excitation is in thermal confinement) and the pressure propagation (i.e., the excitation is in stress confinement) in a heated region, the fractional volume expansion dV/V can be expressed as

$$\frac{dV}{V} = -\kappa p + \beta T,$$

where κ is the isothermal compressibility, β is the thermal coefficient of volume expansion, and p and T denote changes in pressure (measured in Pascal), and temperature (in Kelvin), respectively.

When the fractional change in volume is negligible under rapid heating, the local pressure rise immediately after the microwave/laser excitation pulse can be derived as

$$p_0 = \frac{\beta T}{\kappa} = \frac{\beta}{\kappa \rho C_v} \eta_{th} A_e = \Gamma \eta_{th} A_e,$$

where ρ denotes mass density, C_v denotes specific heat capacity at constant volume, A_e is the specific optical/microwave absorption, and η_{th} is the percentage of absorbed energy that is converted to heat.

We define the Grueneisen parameter (dimensionless) as

$$\Gamma = \frac{\beta}{\kappa \rho C_v} = \frac{\beta \upsilon_s^2}{C_p} = f(T),$$

where υ_s is the velocity of sound, C_p denotes the specific heat capacity at constant pressure, and T is the temperature of the object.

Therefore,

$$p_0 = f(T)\eta_{th} A_e.$$

Thus, in practice, the measured pressure signal generated due to the microwave/laser excitation can be used to monitor temperature. Note that, here we always refer to the base temperature of the object, not the change in temperature due to the microwave/laser heating. The instantaneous temperature increase in the object due to the microwave/laser pulse heating is on the order of milliKelvin and its effect on the Grueneisen parameter is negligible. The base temperature of the object is a slowly varying parameter compared to the transient temperature increase induced by a microwave/laser pulse.
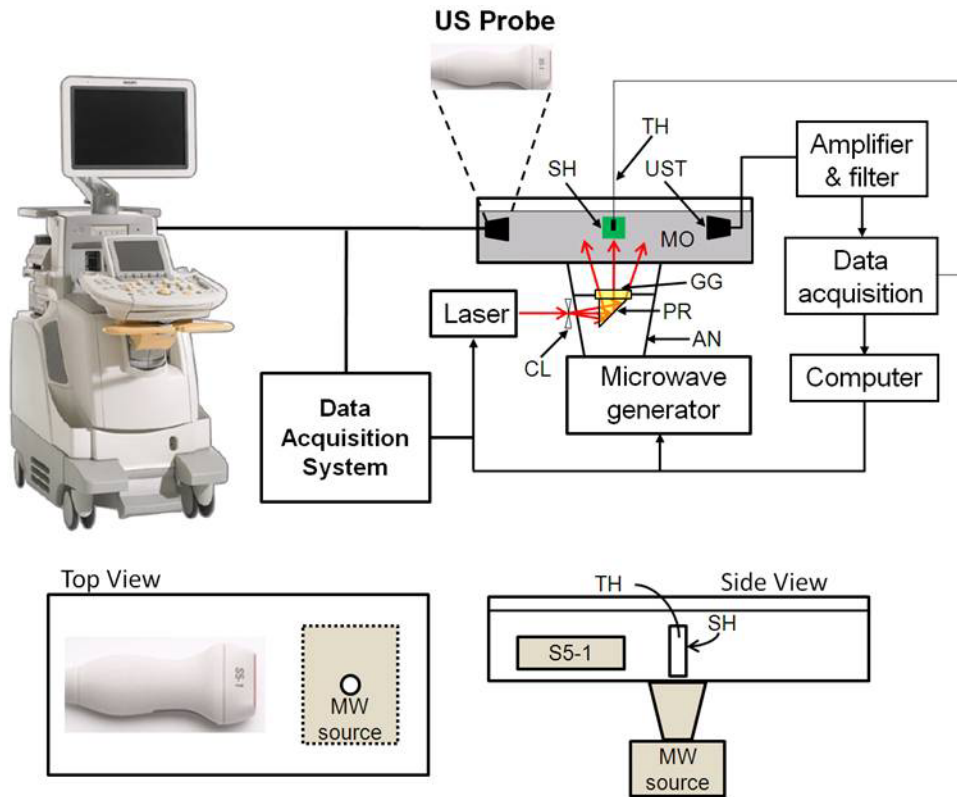
3. SYSTEM DESCRIPTION

Figure 1. Schematic of the experimental setup. Thermoacoustic and photoacoustic imaging system combined with modified Philips iU22 ultrasounds imaging system (Philips healthcare, Andover, MA). MO: mineral oil bath, SH: sample holder vial, UST: single element ultrasonic transducer, GG: ground glass, PR: prism, AN: horn antenna, CL: concave lens, TH: thermistor. Top and side view of the transducer arrangement is also shown.

Figure 1 shows the combined TA and PA system used for sensing temperature with a single element ultrasonic transducer as well as using the Philips iU22 clinical ultrasound imaging system (Philips Healthcare, Andover, MA). A similar concept of integrating light with microwaves was used earlier for a breast cancer imaging system.[21] The plastic chamber containing the sample holder was filled with mineral oil, a nonmicrowave-absorbing material. Moreover, because mineral oil is visibly transparent, light absorption is negligible. Mineral oil also acts as a coupling medium for sound propagation, and thus, mineral oil was an ideal choice as a background medium for all our experiments. The microwave/laser assembly was placed under the sample holder chamber, from where it illuminated the sample by either microwave or laser, alternately, for TA/PA sensing. The microwave was delivered using a horn antenna, whereas the laser was delivered by a free-space optical assembly. The prism and ground glass of the laser illumination system were incorporated inside the microwave horn antenna. As a result, it was not necessary to mechanically switch between the microwave and laser sources: the switching was electronic and instantaneous. Light was delivered through a drilled ~10-mm-diam hole in one of the narrow walls of the horn antenna. The laser beam was broadened by a concave lens placed outside the hole in the horn antenna, then reflected by the prism and homogenized by the ground glass. This type of beam expansion scheme has been used extensively.[13,15,29] The insertion of the optical devices inside the microwave horn antenna had no significant effect on microwave delivery.[21]

3.1 Microwave Source

A 3.0-GHz microwave source produced pulses of 0.5-µs width, with a repetition rate of up to 100 Hz. An air-filled pyramidal horn-type antenna (WR284 horn antenna W/EEV flange, HNL Inc.) with a rectangular opening of 7.3 X 10.7 cm^2 was used to deliver the microwaves to the sample. The specific absorption rate (SAR) of the tissue was within the IEEE safety standards.[30]

The horn antenna was designed to transport the TE_{10} mode of EM waves, so the electric field was parallel (or nearly parallel for a horn) to the surface of either narrow side (y-polarized in our system) and approached zero near the inner surface of either narrow wall. By contrast, the electric field was nonzero near the surface of either wide wall. Therefore, opening the light delivery hole on the narrower side of the horn antenna (or wave guide) minimized the power leakage.

3.2 Laser Source

The light source was a Q-switched Nd:YAG laser with a repetition rate of 10 Hz, providing 6.5-ns-wide laser pulses. The laser system could provide 400-mJ maximal output energy at 532-nm wavelength. The incident laser fluence on the sample surface was controlled to < 20 mJ/cm^2, conforming to the American National Standards Institute (ANSI) safety standards.[31]

3.3 Detection of Ultrasound

For detecting the ultrasound signal, we used two types of detection schemes - one with a single-element transducer and the other based on clinical ultrasound array system.

a) Single-element transducer

We used a 13-mm-diam active-area nonfocused transducer operating at 2.25 MHz central frequency (ISS 2.25 X 0.5 COM, Krautkramer). The signal was first amplified by a low-noise pulse amplifier (5072PR, OlympusNDT), then filtered electronically, and finally recorded using a digital oscilloscope (TDS640A, Tektronix). When microwaves were the illumination source, a delay/pulse generator (SRS, DG535) triggered the microwave pulses and synchronized the oscilloscope. By contrast, during laser illumination, the sync out from the laser system synchronized the laser pulses and the data acquisition.

b) Philips iU22 Ultrasound Imaging System

A one of a kind thermoacoustic and photoacoustic system has been built around a Philips iU22 ultrasound imaging system (Philips Healthcare, Andover, MA).[32] The modified channel board architecture allowed access to raw per-channel thermoacoustic and photoacoustic data, while retaining all imaging capabilities of an actual commercial ultrasound scanner. Raw thermoacoustic, photoacoustic and ultrasound data were transferred to a custom-built data acquisition system for image display and post-processing, providing multi-modality imaging capability. Thermoacoustic and photoacoustic images were reconstructed using a Fourier beamforming algorithm[33] implemented in Matlab (MathWorks Inc., Natick, MA), generating a thermoacoustic and photoacoustic B-mode image from one microwave/laser shot. An FPGA-based electronic board synchronized iU22 data acquisition with the microwave/laser firing. Thermoacoustic data was captured at a frame rate of 50 Hz.

The system can use all standard iU22 array transducers for all three modalities, i.e., thermoacoustic, photoacoustic and ultrasound imaging. The system is capable of using 3 ultrasound array transducers, the phased array S5-1 probe and 2 linear array probes, L8-4 and L15-7 (Philips Healthcare, Andover, MA) with nominal bandwidths of 1-5 MHz, 4-8 MHz, and 7-15 MHz, respectively. These probes span the frequency range typically encountered in clinical diagnostic ultrasound imaging. For this study, we have used S5-1 probe.

3.4 Temperature Sensor

A precision thermistor for laboratory applications (sealed PVC tip, resistance of 2252 Ω at 25 °C and accuracy of ±0.1 °C; ON-401-PP, Omega) was used to measure the temperature of the sample. The tip of the thermistor was inserted inside the sample to get an accurate measurement of the temperature. A voltage divider circuit with a dc source (Vizatek,

MPS-6003L-1) converted the resistance change of the thermistor into voltage, which was recorded using the aforementioned oscilloscope. Because the current through the thermistor was very small, self-heating was negligible.

3.5 Sample holder vial

Low density polyethylene (LDPE) vials with ~12 mm inner diameter and 5 cc volume were the sample holders for the entire study. It was shown in our previous work that the sample holder vial had no detectable effect either in TA or in PA signal generation, and henceforth all signals observed were considered to be generated from the sample placed inside the vial.[28]

3.6 Experimental Procedure

The sample holder vial was filled with different samples, DI water, ink solution, saline, turkey breast tissue. Two types of experiments were done. A heated sample was allowed to come to room temperature by natural convection, exchanging heat with the background medium (mineral oil). The volume of the sample was very small compared to the mineral oil; thus, the temperature rise of the mineral oil was neglected. The TA/PA signal was recorded with time as the sample temperature decreased to room temperature. The thermistor was inserted inside the sample to monitor the actual temperature. Next, a cold sample was allowed to reach room temperature by natural convection, exchanging heat with mineral oil, and the TA/PA signal was recorded with time as the sample temperature increased to room temperature. The actual temperature of the sample was also monitored using a thermistor as before. Note that, for decreasing and increasing temperature experiments, the sample holder position may have altered slightly. The sample holder was removed, refilled with cold/hot sample, and then placed back in the system.

4. RESULTS AND DISCUSSIONS

4.1 Water/ink temperature monitoring using TA/PA measurements with single-element transducer
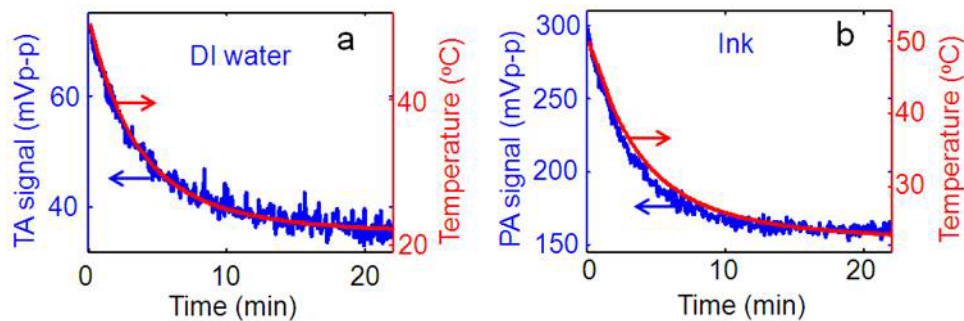

Figure 2. (a) TA signal and actual temperature of DI water as heated DI water was allowed to come to room temperature. (b) PA signal and actual temperature of diluted black ink solution (10 times diluted) as heated sample was allowed to come to room temperature.

Figure 2(a) shows the peak-to-peak TA signal amplitude and the actual temperature of the DI water. The TA signal decreased as the DI water cooled to room temperature with time. The TA signal follows the actual temperature profile (red line) very well. A linear relationship between the actual temperature and the TA signal was observed. For water in this temperature range, the Grueneisen parameter is a linear function of temperature[34,35] and, therefore, the TA signal amplitude also varies linearly with the temperature. Similar experiments were done for PA measurements with ink solution as a sample. Figure 2(b) shows the PA signal generated from the ink solution and the actual temperature. Once again, the PA signal decreased as the solution temperature approached room temperature, and followed the actual

temperature profile (red line) very well. The number of measurements averaged was 20 for each data point, and as the microwave/laser was operating at 10 Hz pulse repetition rate, the temporal resolution was 2 s. We see a 3.9% change in signal amplitude per degree centigrade change in temperature for TA measurements with DI water, and a 3.2% change in PA signal amplitude per degree centigrade change in temperature for PA measurements with ink solution. The TA/PA signal generated from the sample is dependent on various factors such as the orientation of the sample holder and the spatial distribution of microwaves/light on the sample surface. The temperature measurement precision was ±1.2 ^{o}C for TA measurements and ±0.6 ^{o}C for PA measurements. Here, we have used the terms precision and sensitivity synonymously. The temperature precision is calculated based on the uncertainty in the mean value of the measurements (standard error). The precision would improve with the increase of the number of measurements averaged.[28] Note that the precision varies from sample to sample depending on the signal-to-noise (SNR).

4.2 Saline/Tissue temperature monitoring using TA measurements with iU22

Next, we used the iU22 ultrasound system to monitor the temperature of the saline (0.9% w/v of NaCl in water) and turkey breast tissue as a phantom with TA measurements. The same experimental procedures were followed as before, except the S5-1 probe was used to acquire TA signals. Figure 3(a) shows thermoacoustic B-mode image of the vial filled with saline at 50 ^{o}C. Figure 3(b) shows the same cross-section image at 25 ^{o}C after ~25 min. Both a and b are shown in the same colorbar, shown on the right hand side. Visually we can see the hot saline has a higher contrast in the image compared to the room temperature one (marked with white square in a and b). Figure 3(c) shows that the TA signal decreased as the temperature of the saline decreased. The TA signal profile matches very well with the actual temperature profile as measured by the thermistor (red curve). We observed a 4.6% change in TA signal per 1 ^{o}C change in temperature, leading to a ~0.65 ^{o}C temperature sensitivity. The microwave was used with a repetition rate of 10 Hz and 200 measurements were averaged. However, if the SNR is improved the sensitivity could be even better.
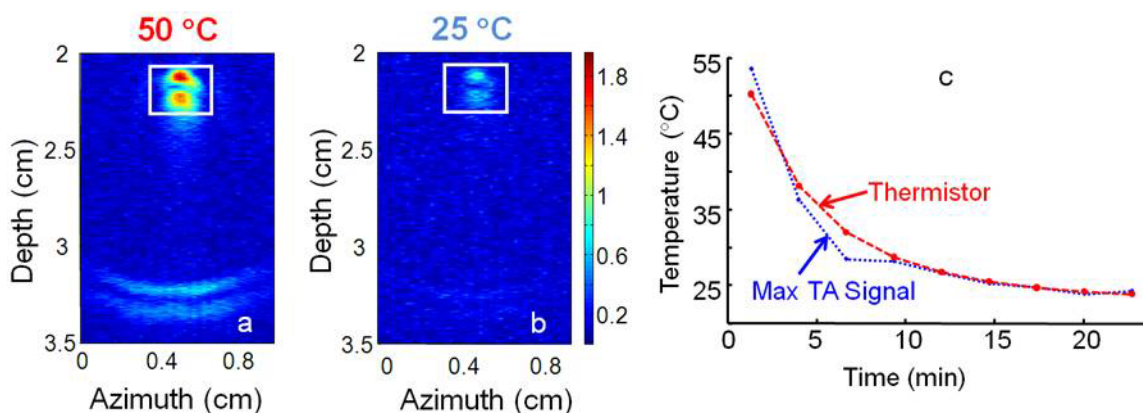

Figure 3. (a) B-mode thermoacoustic image of the vial filled with hot saline. (b) B-mode thermoacoustic image of the same vial when the saline reaches the room temperature (~20 min after a). (c) TA signal and actual temperature of saline as it was allowed to come to room temperature.

Next, we used turkey breast tissue as the sample. Figure 4(a) shows thermoacoustic B-mode image of the vial filled with hot turkey breast tissue at 34 ^{o}C. Figure 3(b) shows the same cross-section image, when the tissue came to equilibrium temperature, i.e., at room temperature (26 ^{o}C), which took ~20 min. Both a and b are shown in the same colorbar, shown on the right hand side. Visually we can see the hot tissue has a higher contrast in the image compared to the room temperature one (marked with white square in a and b). Figure 4(c) shows that the TA signal decreased as the temperature of the tissue decreased. The TA signal profile matches very well with the actual temperature profile as measured by the thermistor (red curve). We observed a 5.9% change in TA signal per 1 ^{o}C change in temperature, leading to a ~0.5 ^{o}C temperature sensitivity. The temperature sensitivity depends primarily on the signal-to-noise ratio, which is affected by numerous factors including transducer bandwidth, overall system amplification, and number of signal averages. Figure 4(d) shows the linear relationship between the temperature and the TA signal amplitude. The red line is a linearly fitted curve. The microwave was used with a repetition rate of 50 Hz and 50 measurements were

averaged. Since the data was acquired in 1 s but data transfer to the hard drive required 2.5 s, a 3.6 s temporal resolution was achieved.
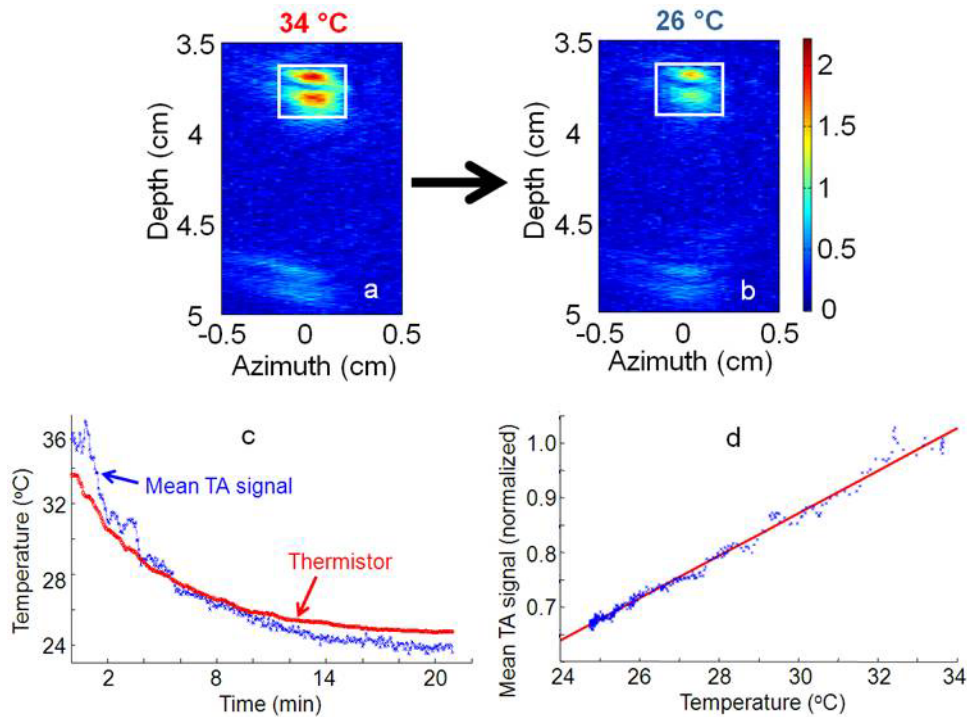

Figure 4. (a) B-mode thermoacoustic image of the vial filled with hot turkey breast tissue. (b) B-mode thermoacoustic image of the same vial when the tissue reaches the room temperature (~20 min after a). (c) TA signal and actual temperature of saline as it was allowed to come to room temperature. (d) Temperature versus the mean TA signal. It follows a linear relationship (red curve shows the linear fit).

Next, the tissue was cooled and allowed to come to room temperature. Figure 5(a) shows thermoacoustic B-mode image of the vial filled with cold turkey breast tissue at 13 °C. Figure 3(b) shows the same cross-section image, when the tissue came to equilibrium temperature, i.e., at room temperature (24 °C), which took ~20 min. Both a and b are shown in the same colorbar, shown on the right hand side. Visually we can see the hot tissue has a higher contrast in the image compared to the room temperature one (marked with white square in a and b). Figure 4(c) shows that the TA signal increased as the temperature of the tissue increased. The TA signal profile matches very well with the actual temperature profile as measured by the thermistor (red curve). We observed a 3.7% change in TA signal per 1 °C change in temperature. Figure 4(d) shows the linear relationship between the temperature and the TA signal amplitude. Red line is a linearly fitted curve. The microwave was used with a repetition rate of 50 Hz and 50 measurements were averaged.
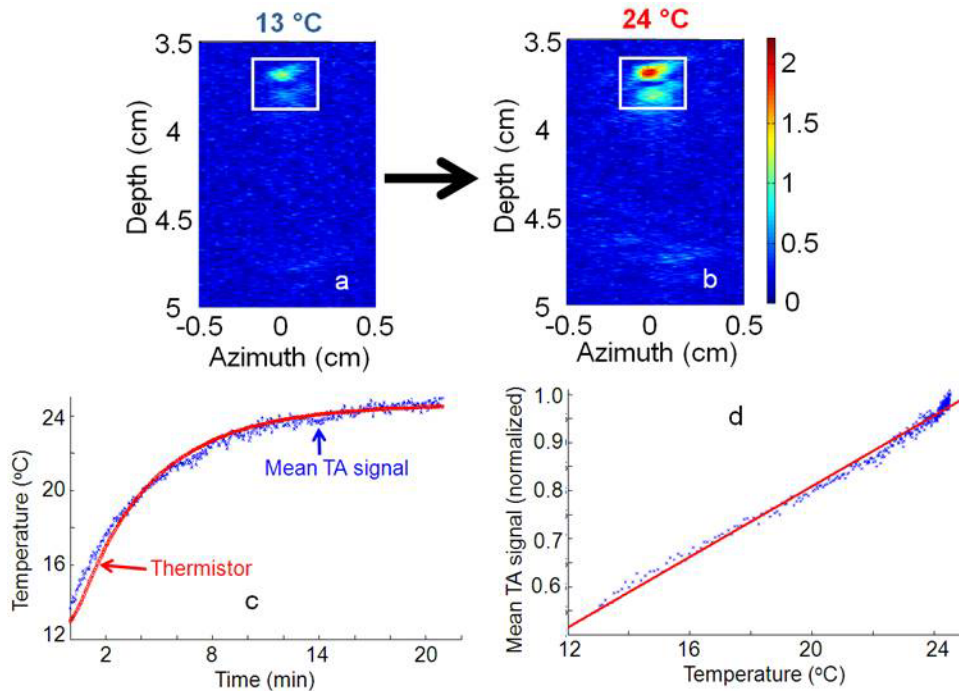
Figure 5. (a) B-mode thermoacoustic image of the vial filled with cold turkey breast tissue. (b) B-mode thermoacoustic image of the same vial when the tissue reaches the room temperature (~20 min after a). (c) TA signal and actual temperature of saline as it was allowed to come to room temperature. (d) Temperature versus the mean TA signal. It follows a linear relationship (red curve shows the linear fit).

5. SUMMARY

A novel temperature sensing method based on TA and PA measurements is reported. This noninvasive method has deep-tissue-sensing capabilities. Depending on the tissue type, either the TA or PA component, or both, could be used. We monitored temperature of DI water thermoacoustically, and temperature of diluted ink solution photoacoustically. We have also shown that a clinical Philips ultrasound imaging system (iU22) can be easily integrated to monitor the temperature of saline and turkey breast tissue using TA-based measurements. The temperature sensitivity was 0.5 $^{\circ}$C with 3.6 s (50 measurements averaged) temporal resolution. Measurement precision could be improved by taking more signal averages. In the future, we would like to continue monitoring temperature *in vivo* using both TA and PA sensing for various applications, such as temperature monitoring for tissue during radiofrequency ablation, radiation therapy, photothermal therapy, photodynamic therapy, cancer treatment using high intensity focused ultrasound (HIFU), and drug delivery using HIFU.

6. ACKNOWLEDGEMENTS

REFERENCES

[1] Larina, I. V., Larin, K. V., and Esenaliev, R. O., "Real-time optoacoustic monitoring of temperature in tissues," Journal of Physics D-Applied Physics, 38, 2633-2639 (2005).

[2] Welch, A. J., and Van Gemert, M. J. C., Optical-Thermal Response of Laser-Irradiated Tissue. New York: Plenum (1995).

[3] Seip, R., and Ebbini, E. S., "Noninvasive Estimation of Tissue Temperature Response to Heating Fields Using Diagnostic Ultrasound," IEEE Transactions on Biomedical Engineering, 42, 828-839 (1995).

[4] MaassMoreno, R., and Damianou, C. A., "Noninvasive temperature estimation in tissue via ultrasound echo-shifts .1. Analytical model," Journal of the Acoustical Society of America, 100, 2514-2521 (1996).

[5] Seip, R., VanBaren, P., Cain, C. A., and Ebbini, E. S., "Noninvasive real-time multipoint temperature control for ultrasound phased array treatments," IEEE Transactions on Ultrasonics Ferroelectrics and Frequency Control, 43, 1063-1073 (1996).

[6] Graham, S. J., Bronskill, M. J., and Henkelman, R. M., "Time and temperature dependence of MR parameters during thermal coagulation of ex vivo rabbit muscle," Magnetic Resonance in Medicine, 39, 198-203 (1998).

[7] Steiner, P., Botnar, R., Dubno, B., Zimmermann, G. G., Gazelle, G. S., and Debatin, J. F., "Radio-frequency-induced thermoablation: Monitoring with T1-weighted and proton-frequency-shift MR imaging in an interventional 0.5-T environment," Radiology, 206, 803-810 (1998).

[8] Hoelen, C. G. A., de Mul, F. F. M., Pongers, R., and Dekker, A., "Three-dimensional photoacoustic imaging of blood vessels in tissue," Optics Letters, 23, 648-650 (1998).

[9] Kruger, R. A., Kopecky, K. K., Aisen, A. M., Reinecke, D. R., Kruger, G. A., and Kiser, W. L., "Thermoacoustic CT with radio waves: A medical imaging paradigm," Radiology, 211, 275-278 (1999).

[10] Wang, L. H. V., Zhao, X. M., Sun, H. T., and Ku, G., "Microwave-induced acoustic imaging of biological tissues," Review of Scientific Instruments, 70, 3744-3748 (1999).

[11] Kruger, R. A., Miller, K. D., Reynolds, H. E., Kiser, W. L., Reinecke, D. R., and Kruger, G. A., "Breast cancer in vivo: Contrast enhancement with thermoacoustic CT at 434 MHz - Feasibility study," Radiology, 216, 279-283 (2000).

[12] Oraevsky, A. A., Savateeva, E. V., Solomatin, S. V., Karabutov, A. A., Andreev, V. G., Gatalica, Z., Khamapirad, T., and Henrichs, P. M., "Optoacoustic Imaging of Blood for Visualization and Diagnostics of Breast Cancer," Proc SPIE 4618, 81-94 (2002).

[13] Wang, X. D., Pang, Y. J., Ku, G., Xie, X. Y., Stoica, G., and Wang, L. H. V., "Noninvasive laser-induced photoacoustic tomography for structural and functional in vivo imaging of the brain," Nature Biotechnology, 21, 803-806 (2003).

[14] Wang, Y. W., Xie, X. Y., Wang, X. D., Ku, G., Gill, K. L., O'Neal, D. P., Stoica, G., and Wang, L. H. V., "Photoacoustic tomography of a nanoshell contrast agent in the in vivo rat brain," Nano Letters, 4, 1689-1692 (2004).

[15] Ku, G., Fornage, B. D., Jin, X., Xu, M. H., Hunt, K. K., and Wang, L. H. V., "Thermoacoustic and photoacoustic tomography of thick biological tissues toward breast imaging," Technology in Cancer Research & Treatment, 4, 559-565 (2005).

[16] Ku, G., Wang, X. D., Xie, X. Y., Stoica, G., and Wang, L. H. V., "Imaging of tumor angiogenesis in rat brains in vivo by photoacoustic tomography," Applied Optics, 44, 770-775 (2005).

[17] Zhang, H. F., Maslov, K., Stoica, G., and Wang, L. H. V., "Functional photoacoustic microscopy for high-resolution and noninvasive in vivo imaging," Nature Biotechnology, 24, 848-851 (2006).

[18] Gamelin, J., Aguirre, A., Maurudis, A., Huang, F., Castillo, D., Wang, L. H. V., and Zhu, Q., "Curved array photoacoustic tomographic system for small animal imaging," Journal of Biomedical Optics, 13, 024007 (2008).

[19] Li, M. L., Oh, J. T., Xie, X. Y., Ku, G., Wang, W., Li, C., Lungu, G., Stoica, G., and Wang, L. H. V., "Simultaneous molecular and hypoxia imaging of brain tumors in vivo using spectroscopic photoacoustic tomography," Proc IEEE, 96, 481-489 (2008).

[20] Song, K. H., Stein, E. W., Margenthaler, J. A., and Wang, L. H. V., "Noninvasive photoacoustic identification of sentinel lymph nodes containing methylene blue in vivo in a rat model," Journal of Biomedical Optics, 13, 054033 (2008).

[21] Pramanik, M., Ku, G., Li, C. H., and Wang, L. H. V., "Design and evaluation of a novel breast cancer detection system combining both thermoacoustic (TA) and photoacoustic (PA) tomography," Medical Physics, 35, 2218-2223 (2008).

[22] De La Zerda, A., Zavaleta, C., Keren, S., Vaithilingam, S., Bodapati, S., Liu, Z., Levi, J., Smith, B. R., Ma, T. J., Oralkan, O., Cheng, Z., Chen, X. Y., Dai, H. J., Khuri-Yakub, B. T., and Gambhir, S. S., "Carbon nanotubes as photoacoustic molecular imaging agents in living mice," Nature Nanotechnology, 3, 557-562 (2008).

[23] Emelianov, S. Y., Aglyamov, S. R., Karpiouk, A. B., Mallidi, S., Park, S., Sethuraman, S., Shah, J., Smalling, R. W., Rubin, J. M., and Scott, W. G., "Synergy and applications of combined ultrasound, elasticity, and photacoustic imaging," Proc IEEE Ultrasound Symp, 405-415 (2006).

[24] Shah, J., Aglyamov, S. R., Sokolov, K., Milner, T. E., and Emelianov, S. Y., "Ultrasound-Based Thermal and Elasticity Imaging to Assist Photothermal Cancer therapy – Preliminary Study," Proc IEEE Ultrason Symp, 1029-1032 (2006).

[25] Sethuraman, S., Aglyamov, S. R., Smalling, R. W., and Emelianov, S. Y., "Remote temperature estimation in intravascular photoacoustic imaging," Ultrasound Med Biol, 34, 299-308 (2008).

[26] Shah, J., Park, S., Aglyamov, S. R., Larson, T., Ma, L., Sokolov, K., Johnston, K., Milner, T. E., and Emelianov, S. Y., "Photoaoustic imaging and temperature measurement for photothermal cancer therapy," Journal of Biomedical Optics, 13, 034024 (2008).

[27] Wang, S. H., Wei, C. W., Jee, S. H., and Li, P. C., "Photoacoustic temperature measurements for monitoring of thermal therapy," Proc SPIE 7177, 71771S (2009).

[28] Pramanik, M., and Wang, L. H. V. "Thermoacoustic and Photoacoustic Sensing of Temperature," Journal of Biomedical Optics 14, 054024 (2009).

[29] Ku, G., and Wang, L. H. V., "Deeply penetrating photoacoustic tomography in biological tissues enhanced with an optical contrast agent," Optics Letters, 30, 507-509 (2005).

[30] IEEE standard for safety levels with respect to human exposure to radio frequency electromagnetic fields 3 kHz to 300 GHz, IEEE Std C95.1, 1999 Edition.

[31] Laser Institute of America, American National Standard for Safe Use of Lasers ANSI Z136.1-2000 (American National Standards Institute, Inc., New York, NY, 2000).

[32] Dean, J., Gornstein, V., Burcher, M., and Jankovic, L., "Real-time photoacoustic data acquisition with Philips iU22 ultrasound scanner," Proc SPIE 6856, 685622 (2008).

[33] Köstli, K., P., Frenz, M., Bebie, H., and Weber, H., P., "Temporal backward projection of optoacoustic pressure transients using fourier transform methods," Physics in Medicine and Biology, 46, 1863-1872 (2001).

[34] Handbook of physical quantities: Boca Raton: CRC Press (1997).

[35] Matthew, J. A. D., Crc Handbook of Chemistry and Physics - Weast,Rc vol. 331 (1988).